

# Soft-X-ray spectra of highly charged Os, Bi, Th, and U ions in an electron beam ion trap

E. Träbert, P. Beiersdorfer, K.B. Fournier, and M.H. Chen

**Abstract:** Systematic variation of the electron-beam energy in an electron-beam ion trap has been employed to produce soft-X-ray spectra of Os, Bi, Th, and U with the highest charge states ranging up to Ni-like ions. Guided by relativistic atomic structure calculations, the strongest lines have been identified with  $\Delta n = 0$  ( $n = 4$  to  $n' = 4$ ) transitions in Rb- to Cu-like ions. The rather weak 4p–4d transitions are much less affected by QED contributions than the dominant 4s–4p transitions. Our wavelength measurements consequently provide benchmarks with and (almost) without QED. Because the radiative corrections are not very sensitive to the number of electrons in the valence shell, our data, moreover, provide benchmarks for the evaluation of electron–electron interactions.

PACS Nos.: 32.30.Rj, 39.30.+w, 31.50.+w

**Résumé :** Nous utilisons une variation systématique de l'énergie du faisceau d'électrons dans un piège à faisceau d'électrons pour produire des rayons-X mous des spectres de Os, Bi, Th et U avec les états de plus haute charge, allant jusqu'aux ions de type Ni. Sur la base de calculs relativistes de structure atomique, les lignes plus intenses ont été identifiées avec les transitions  $\Delta n = 0$  ( $n = 4$  vers  $n' = 4$ ) dans les ions du type Rb jusqu'à Cu. Les transitions plutôt faibles 4p–4d sont beaucoup moins affectées par les corrections QED que les transitions dominantes 4s–4p. En conséquence, nos mesures de longueur d'onde fournissent une référence pour les cas avec et (presque) sans effet QED. Parce que les corrections radiatives ne sont pas très sensibles au nombre d'électrons dans la couche de valence, nos données fournissent aussi une référence pour l'évaluation des interactions électron–électron.

[Traduit par la Rédaction]

## 1. Introduction

A variety of energetic, hot plasmas are of present interest in a range of physical contexts. These encompass controlled fusion experiments based on tokamak discharges, X or Z pinches, high-power laser irradiation of a solid, or intense ion beams striking a nuclear fusion fuel pellet [1–5]. The presence of specific highly charged ions (and thus of electrons abundant and energetic enough to ionize atoms that far) is revealed by the emission of characteristic atomic lines, for example, in the extreme ultraviolet

Received 24 December 2004. Accepted 25 April 2005. Published on the NRC Research Press Web site at <http://cjp.nrc.ca/> on 14 July 2005.

E. Träbert,<sup>1,2</sup> P. Beiersdorfer, K.B. Fournier, and M.H. Chen. High Temperature and Astrophysics Division, Lawrence Livermore National Laboratory, Livermore, CA 94550-9234, USA.

<sup>1</sup>Corresponding author (e-mail: [traebert@ep3.rub.de](mailto:traebert@ep3.rub.de)).

<sup>2</sup>Also at: Fakultät für Physik und Astronomie, Ruhr-Universität Bochum, D-44780 Bochum, Germany.

spectrum. The spectra are then analysed for relative line intensities (in comparison with the predictions of collisional-radiative modeling efforts) to determine electron temperature or density as well as non-Maxwellian electron distribution functions via polarization effects. Moreover, line widths may serve to derive an ion temperature. Beyond the plasma physics and diagnostics value of line, and thus charge state, identifications, precise wavelength data test the available atomic structure codes that for highly charged heavy ions have to take into account large contributions from relativistic effects and notable QED corrections. For a few isoelectronic sequences (mostly with a single electron in the valence shell), precise wavelength data are available now that reach up to uranium ( $Z = 92$ ) (see ref. 6), and some (few) calculations yield a satisfactory match to these data. Theory is struggling, however, with precise descriptions of ions that have more than a single electron in the valence shell [7].

Utilizing a new flat-field EUV spectrometer with higher resolving power than previously available at our facility, we have measured the wavelengths of the resonance lines of Cu- and Zn-like heavy ions [8] with higher precision and accuracy than possible before, confirming the aforementioned systematics of experiment versus calculation. We have now utilized the new spectrometer to observe line emission from charge states lower than nickel-like. The new spectra compare, in range of charge states, to our earlier measurements on the EUV spectra of tungsten (W,  $Z = 74$ ) [9] (which has also been studied at the Berlin electron beam ion trap [10, 11]) and gold (Au,  $Z = 79$ ) [12]. In both cases, the spectral data related to ion species of Rb- to Cu-like isoelectronic sequences. In these spectra, line clusters of prominent lines from a range of neighboring charge states remained unresolved. With the new spectrometer, we have addressed the EUV spectra of highly charged ions of osmium (Os,  $Z = 76$ ), bismuth (Bi,  $Z = 83$ ), thorium (Th,  $Z = 90$ ), and uranium (U,  $Z = 92$ ). In these spectra, we could resolve many 4s–4p transitions that are notably affected by QED contributions, and we also identified a fair number of 4p–4d and 4d–4f transitions that are much less affected by such radiative corrections. Hence, we present benchmarks for calculations of, both, transition energies with and (almost) without QED. Such a twofold set of data has previously been discussed by Simionovici et al. for transitions in the  $n = 3$  shell of highly charged lead ions [13]. Moreover, our data on ions with different numbers of electrons in the valence shell will help to elucidate the electron–electron interaction, which is insufficiently treated in many calculations.

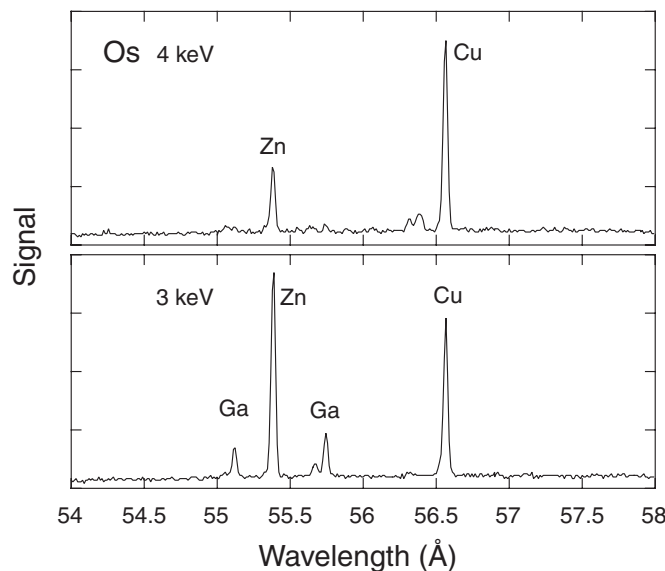
## 2. Experiment

The experiment was set up at the SuperEBIT electron beam ion trap at the University of California Lawrence Livermore National Laboratory. For this low-energy experiment, SuperEBIT was temporarily reconfigured to permit high (100 mA) electron beam currents at relatively low electron-beam energies ( $\geq 4$  keV). Bi, Th, and U ions were introduced into the trap from a metal vapor vacuum arc ion source (MeVVA). This ion source produces ions in low-charge states only. Os was introduced via a ballistic gas injector, using a volatile compound, osmium tetroxide. Highly charged ions are produced from the atoms and ions traveling into the trap volume by multiple collisions with the fast electrons of the high-current density electron beam. Ions become successively better trapped with increasing ion charge. Axial trapping is effected by drift tube potentials, while radial trapping of the ions is due to a combination of the attraction by the electron beam, which also compensates the ion-cloud space charge, and by the very strongly reduced diffusion across the 3 T magnetic guide field. Trapping is considerably aided by bleeding in a light-element gas (we used nitrogen and carbon dioxide, respectively). As the trap is deeper for highly charged ions, ions of the lighter species escape with a higher probability and thus provide evaporative cooling to the remaining ion cloud [14].

The ions were kept inside the trap for 30 to 60 s, then the trap was purged to prevent the accumulation of unwanted heavy contaminants. However, as the build-up phase ( $\leq 1$  s) is included in the observation, the spectrum comprises not only ions of the final charge state distribution (observed under quasi-steady state conditions for most of the cycle), but also lower charge state ions from the initial transient phase.

The light from the trapped ion cloud was observed by a flat-field spectrometer [15] equipped with a variable-line spacing grating (radius  $R = 44.3$  m, approximate line density 2400  $\ell/\text{mm}$ ) and a cryogenic,

**Fig. 1.** Sample spectra of Os in the wavelength range near the 4s–4p resonance lines in the Cu-like ( $\text{Os}^{47+}$ ) and Zn-like ( $\text{Os}^{46+}$ ) ions. The electron-beam energies indicated are rounded and include an estimate of the space charge effect. Labels indicate the dominant charge state component (by isoelectronic sequence) of some of the lines.



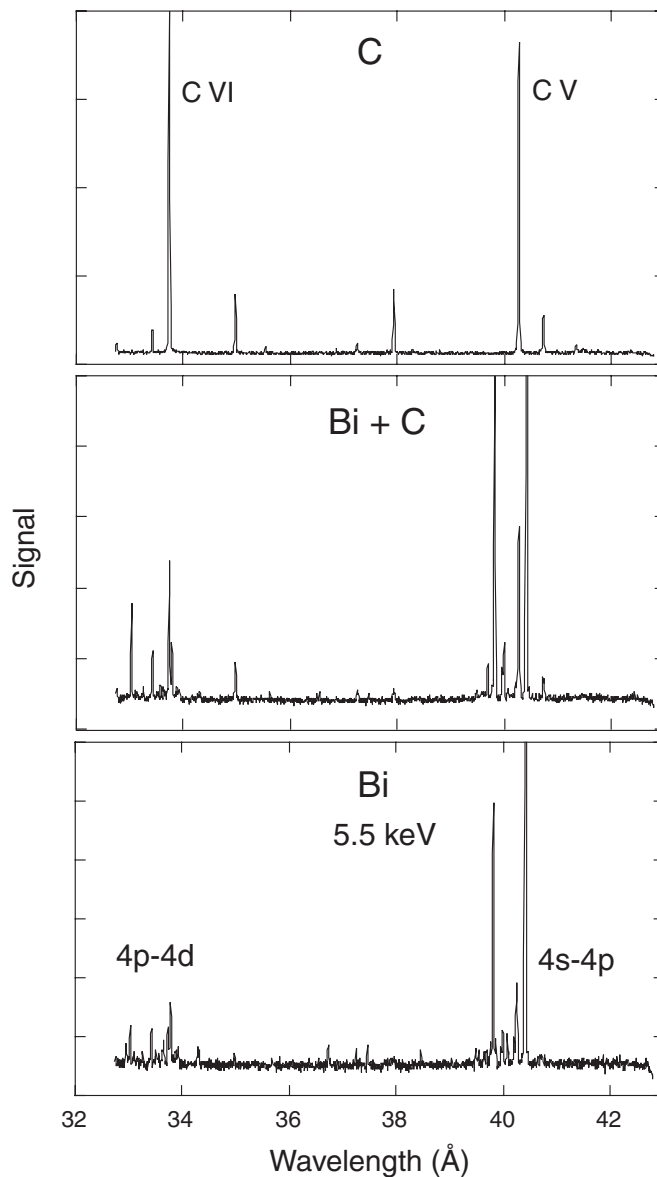
thinned, back-illuminated charge-coupled device (CCD) multichannel detector. Two detectors were used in turn; one had  $1024 \times 1024$  pixels of  $25 \mu\text{m}$  pixel size. Along and across the spectrum some 950 channels were evaluated, cutting out zones of recognized thermal noise problems and spectral line curvature. The other (new) CCD camera had a camera chip of  $1340 \times 1300$  pixels in about the same total area. Line widths (FWHM) (dominated by the width of the light source in our set-up without a spectrometer entrance slit) were about  $0.025 \text{ \AA}$ , which corresponds to about the width of three to four CCD pixels, and a resolving power  $\Delta\lambda/\lambda \approx 1000$  to  $1500$ , depending on the wavelength. The spectral resolution afforded now represents a major improvement (by a factor of up to 5) over the earlier work on W and Au; this improvement was deemed sufficient to disentangle the spectral information.

After filtering for cosmic ray spot events, the raw data were cut down to one narrow central strip (old CCD) or separated into three parallel strips, and the data in each strip were binned along the spectral lines and then analyzed, yielding up to 48 observations of a given ion species at a given electron beam energy. Data on Th and U were collected for various electron beam energies from 4 to 8 keV, in intervals of 200 to 300 eV, thus selecting specific maximum ion charge states up to the Ni-like ions  $\text{Th}^{62+}$  and  $\text{U}^{64+}$ . Os and Bi data were recorded at a few electron beam energies near those optimal for the production of Cu- and Zn-like ions. Eight spectra of Os, 48 spectra of Bi, 72 spectra of Th, and 74 spectra of U were considered to be of sufficient quality to merit evaluation. Sample spectra are shown in Figs. 1–4.

Typical observation times were 20 min (old camera) to 30 min (new camera) per exposure. This is a compromise of long exposure times wanted for a good signal-to-noise ratio on one hand and the need to be able to recognize cosmic-ray events and correct for them on the other; with too many such events in an exposure, the filtering process may be less successful. Repeat exposures at various electron-beam energies ascertained the general reproducibility of the spectral features and their relative intensities.

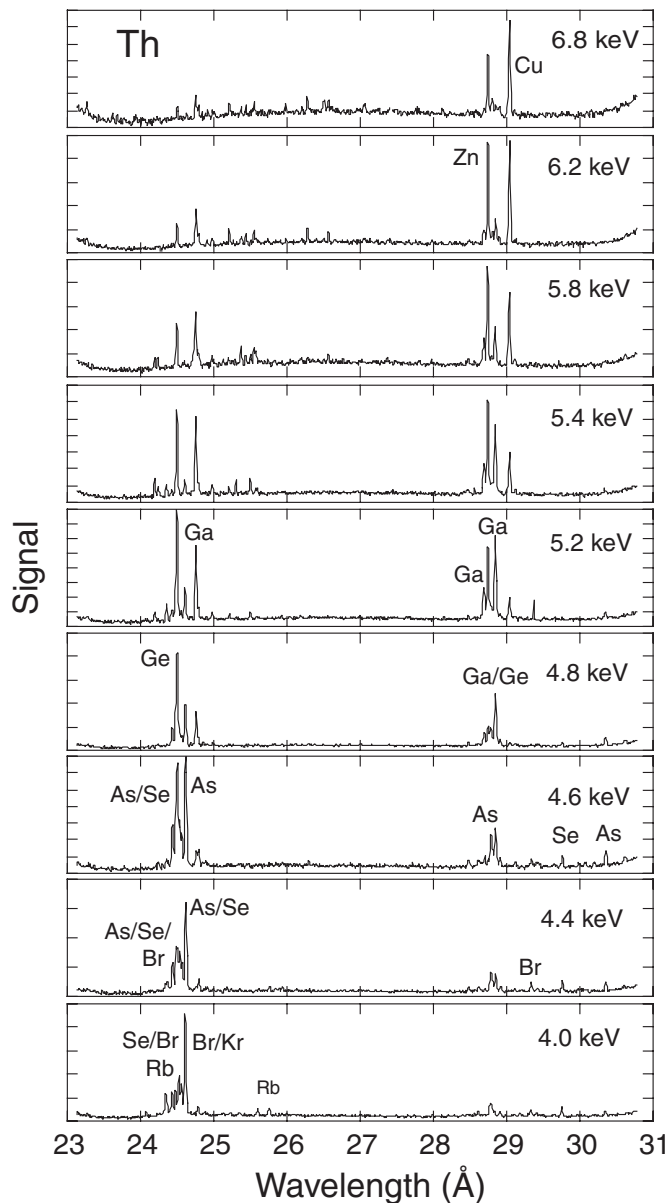
Most of the Th and U spectra were recorded from about 22 to  $30 \text{ \AA}$  in a single exposure (Figs. 3 and 4). They were calibrated with the very well-known  $1s\text{-}np$  transitions in H-like  $\text{C}^{6+}$  ions, and  $1s^2 \text{ } ^1\text{S}_0\text{-}1s2p \text{ } ^1,^3\text{P}_1$  and  $1s^2 \text{ } ^1\text{S}_0\text{-}1s3p \text{ } ^1\text{P}_1$  transitions in He-like ions of N [16–19]. Each of these is known to better than  $1 \text{ m\AA}$ . These lines were produced in dedicated spectra (without Th or U ion injection) at lower electron energies (4 keV) and with short trapping cycles (10 to 30 ms). For the Bi spectra (Fig. 2),

**Fig. 2.** Sample spectrum of Bi (bottom), a calibration spectrum of carbon (top), and a spectrum with simultaneous injection of Bi and C (middle).



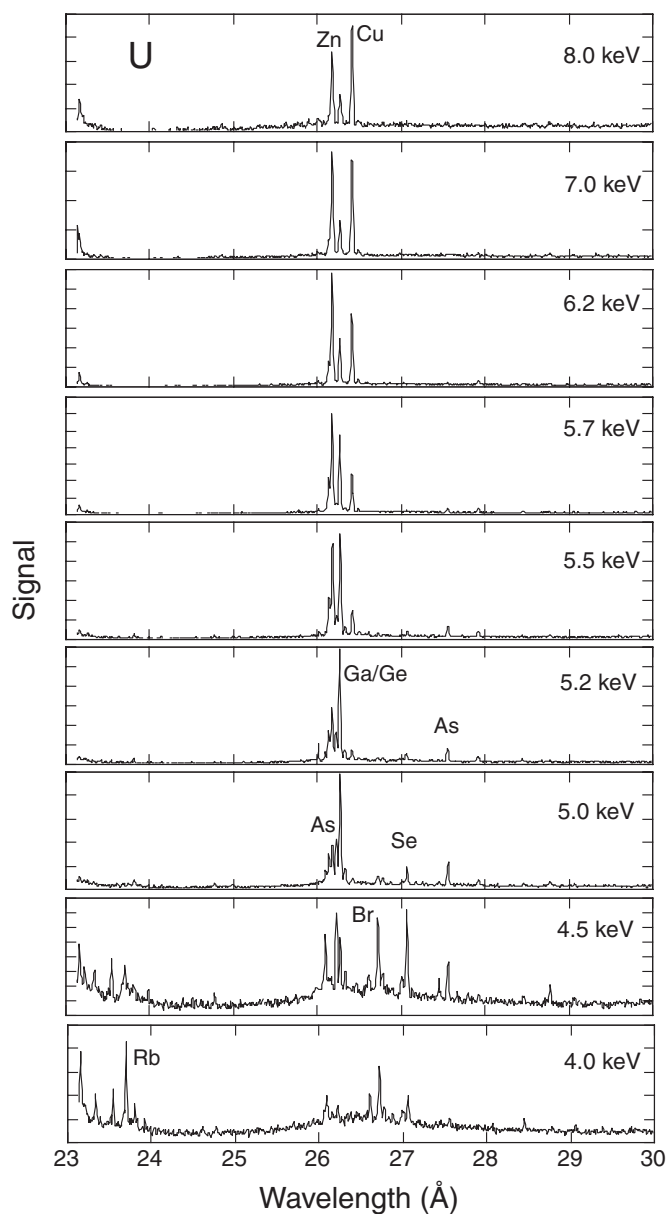
the  $1s-2p$  transitions of  $C^{5+}$  are very close to the line cluster of primary interest. For some spectra of Bi and Th, the  $CO_2$  ( $N_2$ ) cooling gas injection pressure was raised until the calibration lines appeared in the very same spectra as the Bi (Th) lines. While this procedure counters any problems that might arise from instrumental drifts, the problem arises that the calibration lines and some of the lines of interest coincide so closely that least-squares fits are required to disentangle some partial line blends. This problem reduces the precision with which the calibration line positions can be determined in the spectra, and thus the wavelength scale established. Consequently, the uncertainty of the resonance line wavelengths in Cu- and Zn-like Bi is larger than in Th and U. For the calibration of the Os spectra

**Fig. 3.** Sample spectra of Th in the wavelength range 23 to 31 Å. In the lowest-electron-energy spectra, the bulk of the strongest lines arises from charge states lower than Rb-like Th, for which, presently, no calculations are available.



(Fig. 1), nitrogen lines in second-diffraction order were used. However, these lines are not very close to the ones targeted, and this limited the attainable accuracy. The wavelength dispersion was calculated using second- and third-order polynomial fits to the calibration lines.

Most of our calibration spectra were recorded separately, before and after a set of spectra of the element of interest. When bracketing the spectra with about hourly calibrations (and with the aid of enhancing calibration lines in the very spectra of interest), it became possible for some lines to

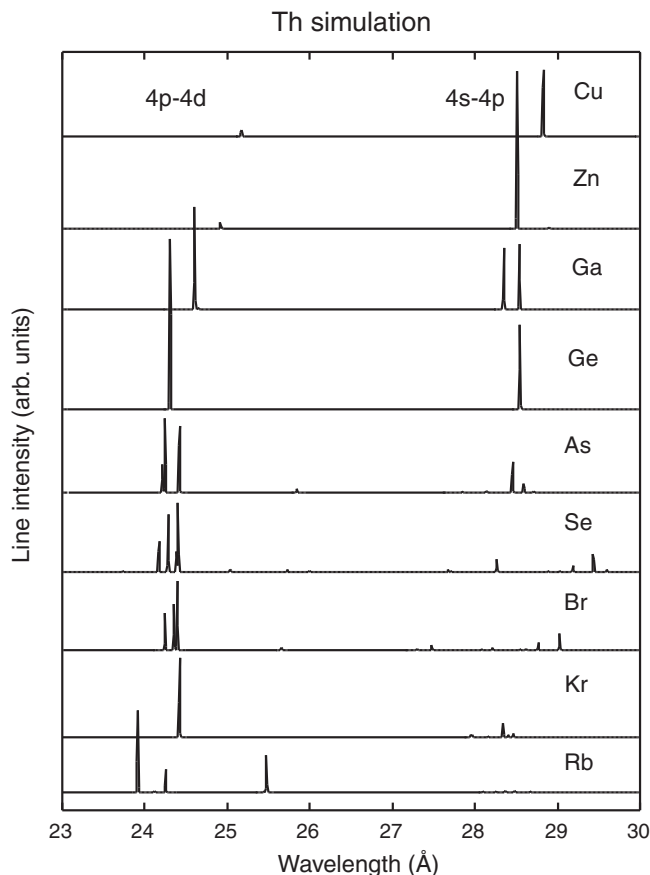
**Fig. 4.** Sample spectra of U in the wavelength range 23 to 30 Å.

reach systematic uncertainties as low as 1 to 2 mÅ. Our wavelength errors represent a combination of systematic and random errors.

### 3. Calculations

The line intensity calculations for Th and U in the present work followed the example of calculations for W that have been published elsewhere [20, 21] and that for Au were incorporated in our earlier study [12].

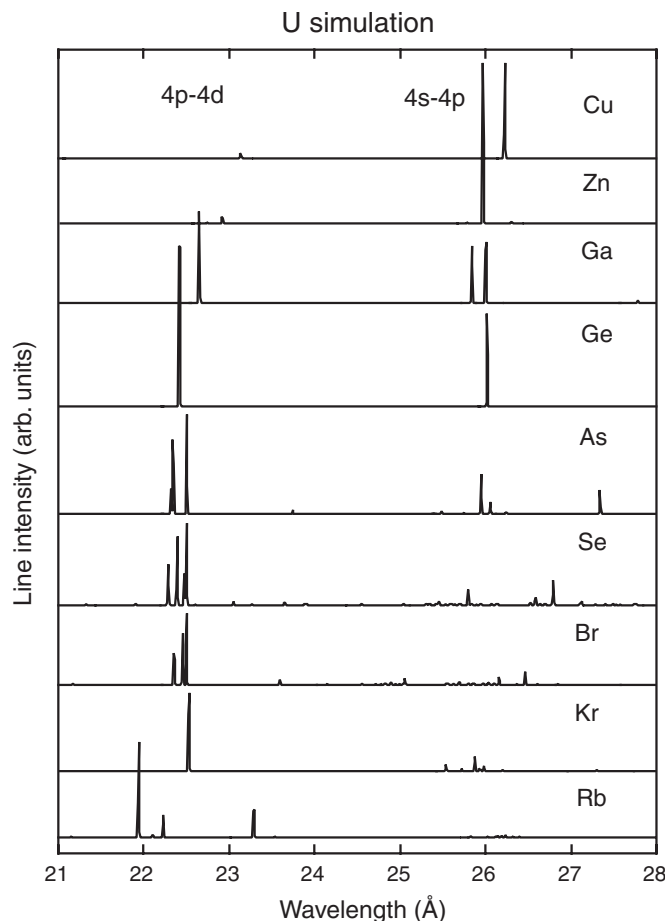
**Fig. 5.** Collisional-radiative synthetic spectra for Rb-like  $\text{Th}^{53+}$  to Cu-like  $\text{Th}^{61+}$ . All calculations assume an electron beam energy of 4.0 keV. The 4s–4p and 4p–4d transitions in ions of several charge states form distinctive line clusters.



Synthetic collisional-radiative spectra were computed for  $\text{Th}^{53+}$  to  $\text{Th}^{61+}$ , and for  $\text{U}^{55+}$  to  $\text{U}^{63+}$ , that is, for the Rb- to Cu-like spectra in the present experiment. For Os and Bi, only spectra of the Ge- to Cu-like ions were generated ( $\text{Os}^{44+}$  to  $\text{Os}^{47+}$  and  $\text{Bi}^{51+}$  to  $\text{Bi}^{54+}$ ). The atomic data used in the simulation of the spectra were generated with the HULLAC suite of codes [22]. Energy levels and E1, E2, M1, and M2 transition rates were computed with the fully relativistic parametric potential code RASER [22]. Cross sections for the electron impact excitation of bound electrons were computed semi-relativistically in the distorted wave approximation (DWA). All possible  $\Delta n = 0$  (4–4) and  $\Delta n > 0$  (3–4, 3–5, and 4–5) excitations between singly excited levels were considered. Some doubly excited configurations were included in the models to account for configuration interaction as fully as possible. Since the electron beam ion trap employs a quasi-monoenergetic electron beam, the calculations were done at a given energy, assuming a Gaussian energy spread with a FWHM of 50 eV. In our earlier work, the relative strengths of the emission features in each ion have been found to be nearly the same in such simulations when assuming either a quasi-monoenergetic electron beam (as done here) or a Maxwellian energy distribution.

The DWA cross sections were integrated over the distribution of free electron energies to determine the final impact excitation rate coefficients. The electron impact excitation rate coefficients and the radiative transition probabilities were then entered into the collisional-radiative rate matrix. The steady-state relative populations for the levels of each ion were found by solving a coupled set of rate equations.

**Fig. 6.** Collisional-radiative synthetic spectra for Rb-like  $U^{55+}$  to Cu-like  $U^{63+}$ . The calculations assume electron beam energies in the range from 4.0 to 5.0 keV.

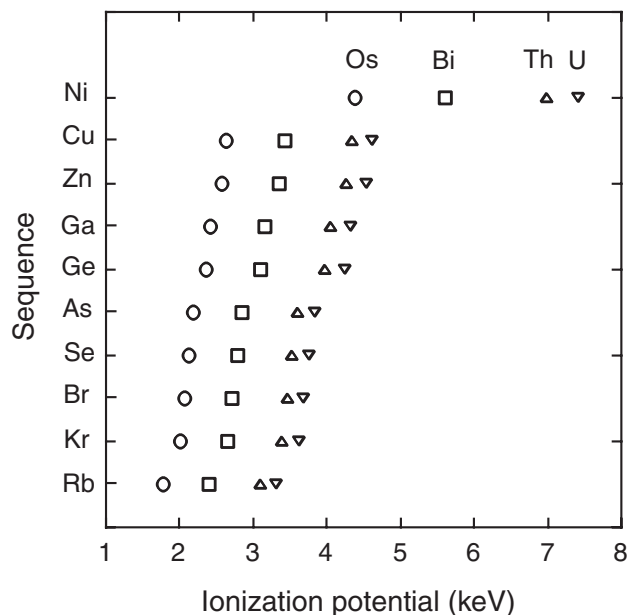


All electric and magnetic dipole and quadrupole radiative transitions as computed by HULLAC were taken into account. Previous work with W spectra from these charge states has shown that electric-dipole-forbidden transitions in this spectral range can be quite bright for the temperature and density conditions of the present experiments [20,21]. The results of the calculations for Th and U are summarized in Figs. 5 and 6.

The present HULLAC calculations aimed simply at providing a guideline for the identification of the strongest (expected) lines of each ion by delivering estimates of wavelengths and of relative intensities of neighboring lines. At the lower electron beam energies, strong lines appear that evidently are from lower charge-state ions than those modeled here.

The HULLAC code provides wavelength data with limited accuracy. However, very accurate calculations of the 4s–4p transitions are available for Cu-like ions that include QED corrections to first and second order [23]. The results of these calculations agree with our aforementioned measurements [8]. The QED contributions are much smaller (but still notable) in the 4p–4d transitions that have not yet been covered in similar detail. We have, therefore, carried out large-scale relativistic configuration interaction (RCI) calculations of the 4p–4d transitions in Cu-like ions. The calculations are based on the no-pair Hamiltonian including Coulomb and Breit interactions. We used finite B-spline basis functions that are solutions of the Dirac equation for an electron moving in a Dirac–Kohn–Sham (DKS) potential

**Fig. 7.** Ionization potentials<sup>3</sup> of ions of various isoelectronic sequences (left axis) of the elements of present interest. Symbols used to label different elements are identified for Ni-like ions.



confined to a finite cavity. The CI expansion included states from all the possible configurations that arise from excitation up to one electron from the Ni-like core and up to one electron from the valence shell [24]. In this work, QED corrections were calculated from the one-loop self energy and vacuum polarization diagrams using appropriate DKS potentials that correspond to the initial and final states to account for the relaxation effects. We also included the mass polarization corrections (MP) obtained as the expectation values of the MP operator using RCI eigenvectors [24,25]. Details for these calculations will be reported elsewhere.

#### 4. Data and discussion

The ionization potentials of Rb- to Cu-like ions of the elements studied here lie in an interval of about 1 keV for each element (1.79 to 2.63 keV for Os, 2.40 to 3.42 keV for Bi, 3.39 to 4.34 keV for Th, 3.62 to 4.63 keV for U,<sup>3</sup> see Fig. 7). In the electron beam ion trap a given open-shell charge state reaches its maximum abundance several hundred eV above the threshold for ionization of its neighboring, lower charge state. The charge-state distribution begins to decline at electron beam energies at which further ionization depletes the previously highest charge states in favor of even higher ones. Therefore, the development of the charge state distribution and the appearance and disappearance of lines in the spectrum are very systematically tied to the electron beam energy. However, with ionization potentials so closely spaced, it is not unequivocally predictable at which electron beam energy which ion species begins to show clearly in the spectra.

Cu- and Zn-like ions (in this wavelength range) can be investigated most precisely, because they have prominent 4s–4p resonance lines, and the ions can be prepared at the cost of most lower charge states as long as the electron beam energy remains low enough not to ionize beyond the Ni-like ion charge state. (The ionization potential of Ni-like ions with their closed-shell ground configuration is relatively high. The resonance lines of Ni-like ions, therefore, also lie in a different wavelength range.)

<sup>3</sup>J.H. Scofield. Private communication.

**Table 1.** Line identifications and measured wavelengths (in Å) for Os, Bi, Th, and U ions. The identifications are based on observed production thresholds and on available calculations. *bl* lines blended with others. The uncertainty of the measured wavelengths is given in parentheses.

Isoel. sequence	Transition	Ion	Ion	Ion	Ion
Cu	$3d^{10}4p\ J = 1/2 - 3d^{10}4d\ J' = 3/2$	Os <sup>47+</sup>	Bi <sup>54+</sup>	Th <sup>61+</sup>	U <sup>63+</sup>
	$3d^{10}4s\ J = 1/2 - 3d^{10}4p\ J' = 3/2$	56.5630(20)	40.4066(20)	25.203(5)	23.168(2)
Zn	$3d^{10}4s4p\ J = 1 - 3d^{10}4s4d\ J' = 2$	Os <sup>46+</sup>	Bi <sup>53+</sup>	Th <sup>60+</sup>	U <sup>62+</sup>
	$3d^{10}4s^2\ J = 0 - 3d^{10}4s4p\ J' = 1$	55.3840(50)	39.8151(20)	24.980(5)	22.974(3)
Ga	$4s^24p\ J = 1/2 - 4s^24d\ J' = 3/2$	Os <sup>45+</sup>	Bi <sup>52+</sup>	Th <sup>59+</sup>	U <sup>61+</sup>
	$4s^24p\ J = 1/2 - 4s4p^2\ J' = 1/2$	55.123(6)	39.690(3)	24.747(5)	22.778(3)
	$4s^24p\ J = 1/2 - 4s4p^2\ J' = 3/2$	55.741(5)	39.991(3)	28.677(3)	26.147(3)
Ge	$4s^24p^2\ J = 0 - 4s^24p4d\ J' = 1$	Os <sup>44+</sup>	Bi <sup>51+</sup>	Th <sup>58+</sup>	U <sup>60+</sup>
	$4s^24p^2\ J = 0 - 4s4p^3\ J' = 1$	55.665(5)	39.955(3)	24.487(5)	22.559(3)
As	$4s^24p^3\ J = 3/2 - 4s^24p^24d\ J' = 1/2, 3/2, 5/2$			Th <sup>57+</sup>	U <sup>59+</sup>
	$4d\ J = 5/2 - 4f\ J' = 5/2, 7/2$			24.602(5) bl	bl
	$4s^24p^3\ J = 3/2 - 4s4p^4\ J' = 3/2$			28.776(5)	26.235(5)
	$4s^24p^3\ J = 3/2 - 4s4p^4\ J' = 5/2$				26.341(5)
Se	$4s^24p^4\ J = 2, 0, 2 - 4s^24p^34d\ J' = 2, 1, 3$			Th <sup>56+</sup>	U <sup>58+</sup>
	$4s^24p^4\ J = 2 - 4s4p^5\ J' = 2$			24.602(5) bl	26.104(5) bl
	$4s^24p^4\ J = 2 - 4s4p^5\ J' = 1$			28.615(10)	26.787(5)
Br	$4s^24p^5\ J = 3/2 - 4s^24p^44d\ J' = 1/2, 5/2, 3/2$			29.739(5)	27.078(5)
	$4s^24p^5\ J = 3/2 - 4s^24p^44d\ J' = 5/2, 3/2$			Th <sup>55+</sup>	U <sup>57+</sup>
Kr	$4s^24p^6\ J = 0 - 4s^24p^54d\ J' = 1$			bl	bl
				29.326(5)	26.730(5)
Rb	$4s^24p^64d\ J = 3/2 - 4s^24p^54d^2\ J' = 1/2$			Th <sup>54+</sup>	U <sup>56+</sup>
				bl	bl
				Th <sup>53+</sup>	U <sup>55+</sup>
				bl	23.550(5)

The technical conditions of the “low-energy mode” SuperEBIT favored operation at 4 keV and above. This implies that, for Th and U, a high electron beam current was available for observations starting several hundred eV below the ionization energies of the Zn-like and Cu-like ions. In the electron beam energy range thus available, lines from successively higher charge states show up with increased beam energy, grow, and decline (Figs. 3 and 4). The lowest charge states of which we identified lines are Rb-like ions. For Os and Bi, in contrast, the low-energy SuperEBIT mode made it difficult to obtain a strong electron beam at energies lower than the ionization energies of Zn-like and Cu-like ions, and we did not pursue the investigation into this regime. Here, the lowest charge states studied were Ge-like ions. Line assignment was guided by the simulated spectra as well as by the step-by-step comparison of spectra recorded with different electron beam energies. The results of this effort are listed in Table 1.

Our spectral calculations are adequate to identify the strongest lines with transitions in Th and

**Table 2.** Comparison of calculated and measured energies of the  $4p_{1/2}$ – $4d_{3/2}$  transition in Cu-like ions. The calculated contributions (RCI, mass polarization MP, and relaxed-core QED) to the total energy are listed separately. The HULLAC wavelengths are also listed.

Ion	Energy			Total ( RCI + MP + QED ) (eV)	Wavelength		
	RCI (eV)	MP (eV)	QED (eV)		Measurement (Å)	HULLAC (Å)	
Bi <sup>54+</sup>	367.323	−0.05861	−0.267	366.997	33.784	33.7855(20)	33.768
Th <sup>61+</sup>	492.559	−0.07918	−0.491	491.989	25.201	25.203(5)	25.177
U <sup>63+</sup>	535.837	−0.08653	−0.582	535.168	23.167	23.168(2)	23.142

U ions of various charge states. The mismatch of HULLAC calculational result and measured  $4s$ – $4p$  transition wavelength is smallest (about 0.5% or 130 mÅ) for Cu- and Zn-like ions. For comparison, most of our observations are accurate to 2–5 mÅ. The mismatch clearly increases for ions of the Ga isoelectronic sequence and beyond. Taking the ions studied here and the present HULLAC calculations as examples, theory is less accurate than our new experiments by a factor of about 20 to 50. The level of agreement reported on here is typical of HULLAC predictions for  $\Delta n = 0$  transition wavelengths. HULLAC calculations are adequate for most modeling efforts, and they are very helpful as an aid to spectral analysis. However, the calculational predictions clearly fall short of spectroscopic accuracy. Now that reference data are available even for the highest- $Z$  natural elements, calculations for elements not covered here or in the precursor experiments can be scaled semiempirically, and such results should be sufficient for many purposes. Nevertheless, the precision of our data on a number of ions that differ by the number of valence electrons provides an incentive to improve on the accuracy of calculations for ions with more than a single valence electron.

For the  $4s$ – $4p$  transitions, there is a notable radiative correction of several eV (about 3.05 eV for U<sup>63+</sup> [23]). The QED contribution is mostly associated with the  $4s$  electron. The various  $4s$ – $4p$  transitions thus feature rather similar QED contributions to the transition energy. Calculations are very good for Cu-like ions as shown earlier [8]. As mentioned before, the agreement is progressively poorer for Zn-like, Ga-like, Ge-like ions, and so on. This is not a matter of the QED calculation, but mostly reflects the complexity of the non-QED part of the calculation, notably of the electron–electron interaction in the valence shell.

The relative importance of QED can be assessed by looking at the  $4p$ – $4d$  and  $4d$ – $4f$  transitions. These are less affected by radiative corrections. In Table 2, we present a comparison of our measurements of the  $4p_{1/2}$ – $4d_{3/2}$  transition in Cu-like Bi, Th, and U with our HULLAC calculations and with those using the RCI method augmented by separate QED calculations. The QED contribution to the transition energy is about 0.58 eV or 28 mÅ for the  $4p_{1/2}$ – $4d_{3/2}$  transition in Cu-like U (Table 2). This is of the same order of magnitude as the mismatch between the HULLAC calculations and our measurements in this case, but is much smaller than the mismatch of the HULLAC results and our experimental findings on  $4s$ – $4p$  transitions in ions with more than one valence electron. We note that the RCI calculations provide an excellent match to the measured values for the  $4p_{1/2}$ – $4d_{3/2}$  transition wavelength in Cu-like ions. This good match is achieved with the “relaxed-core” QED model. Unfortunately, RCI calculations for the transitions of the lower charge-state ions are not readily available because of the prohibitive computational effort required at present.

A very practical problem is suggested by the simulated spectra from our present calculations (Figs. 5 and 6), and this suggestion is borne out to an even higher degree by our observations (Figs. 2, 3, and 4). The simulated spectra show that lines from the  $4s$ – $4p_{3/2}$  transitions and from the  $4p$ – $4d$  transitions in several charge states cluster in (separate) narrow wavelength intervals. The predicted line spacings are comparable to the differential uncertainty of the prediction, disallowing the immediate identification of many lines or even identification with an ion of a given charge state. Moreover, the spectra show several strong lines that even at our rather high resolution do not show a notable substructure or significant

broadening beyond the instrumental width, although they must contain contributions from ions of different charge states (Ga- and Ge-like ions, Ga/As/Se, As/Se/Br). This situation of several near-perfect spectral blends is reflected in the excitation curves. Our spectra also show a multitude of quite reproducible, but presently unassignable weak lines. Last, but not least, at our lowest electron beam energies, the spectra are populated with a multitude of lines from ions in lower charge states than have been calculated and analyzed here. Sufficiently accurate calculational predictions as are necessary for line identifications in these spectra are not yet in sight.

## Acknowledgement

Technical support by E.W. Magee, M. Lawrence, and P. D'Antonio is gratefully acknowledged. ET benefits from travel support from the German Research Association (DFG). K.T. Cheng is thanked for undertaking the QED calculations of Cu-like ions on request. This project was performed under the auspices of the US Department of Energy by the University of California Lawrence Livermore National Laboratory under Contract No. W-7405-Eng-48.

## References

1. S. von Goeler, P. Beiersdorfer, M. Bitter J. Phys. (Paris) Coll. C1, Suppl. au n° 3, **49**, C1-181 (1988).
2. E. Hinnov, P. Beiersdorfer, R. Bell, J. Stevens, S. Suckewer, S. von Goeler, and A. Wouters. Phys. Rev. A, **35**, 4876 (1987).
3. M.E. Foord, S.H. Glenzer, R.S. Thoe, K.L. Wong, K.B. Fournier, J.R. Albritton, B.G. Wilson, and P.T. Springer. J. Quantum Spectrosc. Radiat. Transfer, **65**, 231 (2000).
4. S.H. Glenzer, K.B. Fournier, B.G. Wilson, R.W. Lee, and L.J. Suter. Phys. Rev. Lett. **87**, 045002 (2001).
5. A. Shlyaptseva, D. Fedin, S. Hamasha Rev. Sci. Instrum. **75**, 3750 (2004).
6. S.B. Utter, P. Beiersdorfer, E. Träbert, and E.J. Clothiaux. Phys. Rev. A, **67**, 032502 (2003).
7. S.B. Utter, P. Beiersdorfer, and E. Träbert. Can. J. Phys. **81**, 911 (2003).
8. E. Träbert, P. Beiersdorfer, and H. Chen. Phys. Rev. A, **70**, 032506 (2004).
9. S.B. Utter, P. Beiersdorfer, and E. Träbert. Can. J. Phys. **80**, 1503 (2002).
10. C. Biedermann, R. Radtke, J.-L. Schwob, P. Mandelbaum, R. Doron, T. Fuchs, and G. Fußmann. Phys. Scr. T, **92**, 85 (2001).
11. R. Radtke, C. Biedermann, J.-L. Schwob, P. Mandelbaum, and R. Doron. Phys. Rev. A, **64**, 012720 (2001).
12. E. Träbert, P. Beiersdorfer, K.B. Fournier, S.B. Utter, and K.L. Wong. Can. J. Phys. **79**, 153 (2001).
13. A. Simionovici, D.D. Dietrich, R. Keville, T. Cowan, P. Beiersdorfer, M.H. Chen, and S.A. Blundell. Phys. Rev. A, **48**, 3056 (1993).
14. M.B. Schneider, M.A. Levine, C.L. Bennett, J.R. Henderson, D.A. Knapp, and R.E. Marrs. In International Symposium on Electron Beam Ion Sources and their Applications. Upton, NY 1988, AIP Conference Proceedings No. 188, Edited by A. Hershcovitch. AIP, New York. 1989. p. 158
15. P. Beiersdorfer, E.W. Magee, E. Träbert, H. Chen, J.K. Lepson, M.-F. Gu, and M. Schmidt. Rev. Sci. Instrum. **75**, 3723 (2004).
16. J.D. Garcia and J.E. Mack. J. Opt. Soc. Am. **55**, 654 (1965).
17. G.W.F. Drake. Can. J. Phys. **66**, 586 (1988).
18. L. Engström and U. & Litzén. J. Phys. B: At. Mol. Opt. Phys. **28**, 2565 (1995).
19. R.L. Kelly. On-line data base at <http://cfa-www.harvard.edu/amdata/ampdata/kelly/kelly.html>
20. K. Asmussen, K.B. Fournier, J.M. Laming, R. Neu, J.F. Seely, R. Dux, W. Engelhardt, J.C. Fuchs, and ASDEX Upgrade Team. Nucl. Fusion, **38**, 967 (1998).
21. K.B. Fournier. At. Data Nucl. Data Tables, **68**, 1 (1998).
22. A. Bar-Shalom, M. Klapisch, and J. Oreg. J. Quantum Spectrosc. Radiat. Transfer, **71**, 169 (2001).
23. S.A. Blundell. Phys. Rev. A, **47**, 1790 (1993).
24. M.H. Chen, K.T. Cheng, W.R. Johnson, and J. Sapirstein. Phys. Rev. A, **52**, 266 (1995).
25. K.T. Cheng, W.R. Johnson, and J. Sapirstein. Phys. Rev. A, **47**, 1817 (1993).